Inorganic Chemistry

including bioinorganic chemistry

April 15, 2013
Volume 52, Number 8
pubs.acs.org/IC

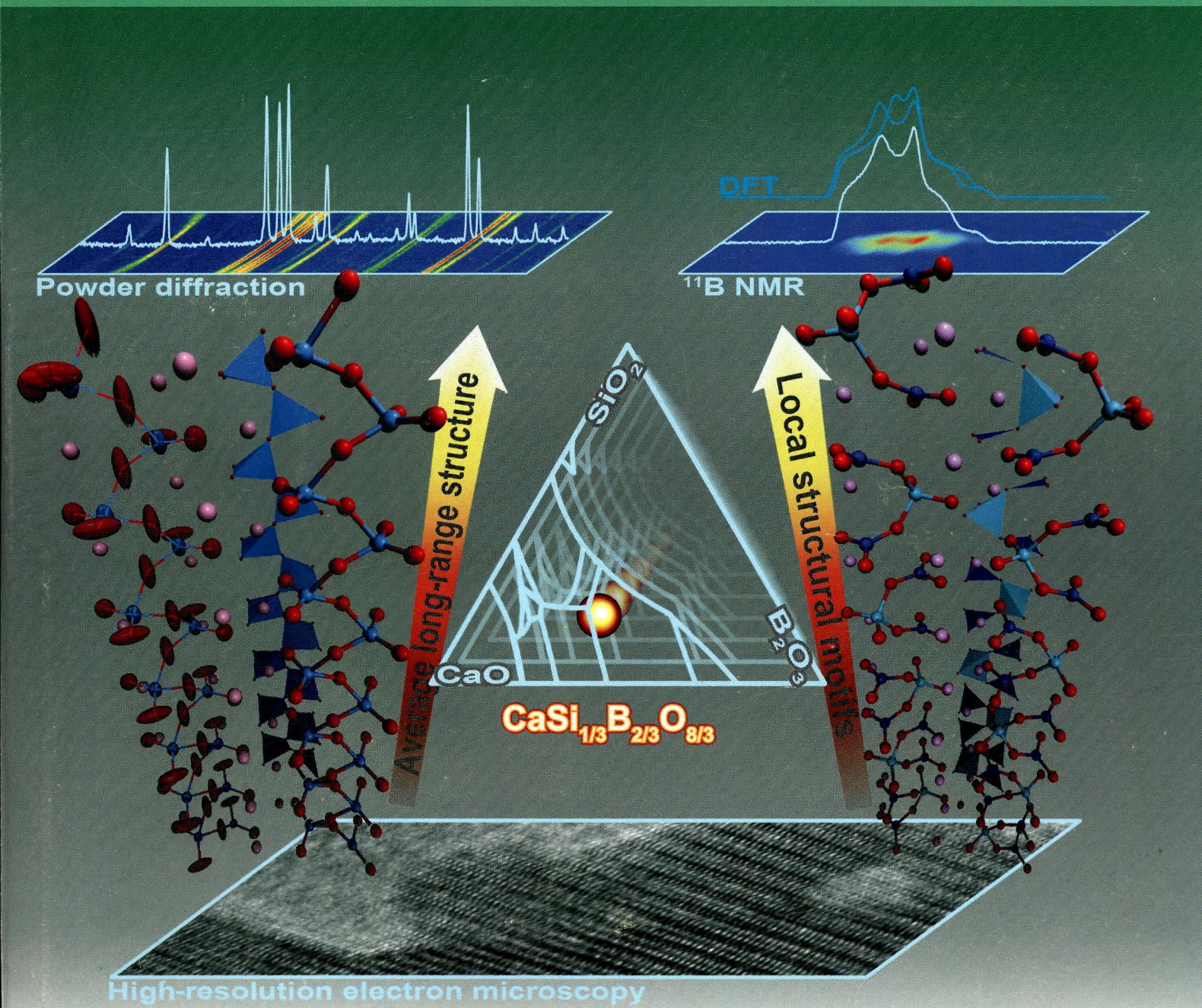

ACS Publications
MOST TRUSTED. MOST CITED. MOST READ.

www.acs.org

Inorganic Chemistry

APRIL 15, 2013
VOLUME 52 ISSUE 8
INOCAJ 52(8) 4121–4746 (2013)
ISSN 0020-1669
Registered in the U.S. Patent and Trademark Office

ON THE COVER: The crystal structure of a new calcium borosilicate compound, $CaSi_{1/3}B_{2/3}O_{8/3}$, is solved ab initio from powder diffraction data collected in situ at high temperature, and the local environments of both boron and silicon species are specified by solid-state NMR spectroscopy. The structure is composed of finite chains built up from SiO_4 tetrahedra and BO_3 trigonal planar coordination units and interestingly exhibits short-range ordering at nanometer scale, as revealed by high-resolution transmission electron microscopy. See E. Véron, M. N. Garaga, D. Pelloquin, S. Cadars, M. Suchomel, E. Suard, D. Massiot, V. Montouillout, G. Matzen, and M. Allix, p 4250.

Communications

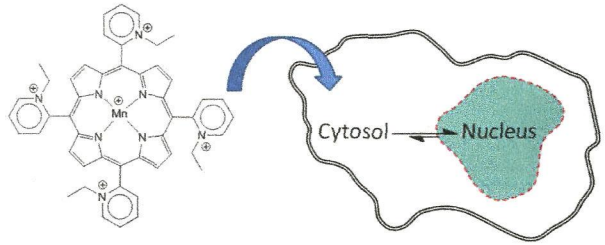

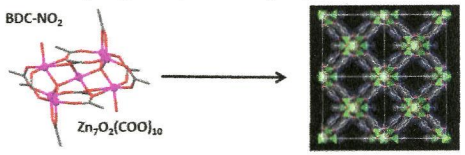

4127 S dx.doi.org/10.1021/ic3025183

Serendipitous Assemblies of Two Large Phosphonate Cages: A Co_{15} Distorted Molecular Cube and a Co_{12} Butterfly Type Core Structure

Javeed Ahmad Sheikh, Soumyabrata Goswami, Amit Adhikary, and Sanjit Konar*

This work describes the solvothermal synthesis, magnetic, and structural characterization of two novel transition metal cages. Both molecules were synthesized by a very similar method. Change in molar conc. of the coligand (from 1 to 0.5 mmol) in the synthesis resulted in two different cage complexes. New types of geometry of the metal–oxo inorganic cores are reported for the first time for these complexes. The symmetry features found in the nuclei may provide new models in single molecular magnetic materials.

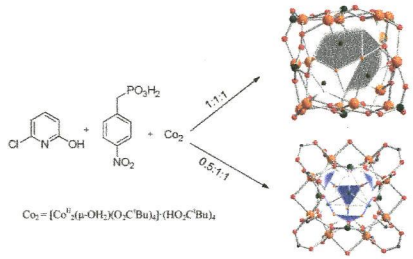

4130 S dx.doi.org/10.1021/ic400296b

Self-construction of Magnetic Hollow $La_{0.7}Sr_{0.3}MnO_3$ Microspheres with Complex Units

Xuefeng Chu, Keke Huang, Mei Han, and Shouhua Feng*

The architecture process of $La_{0.7}Sr_{0.3}MnO_3$ microstructure hollow spheres prepared by a hydrothermal method is shown.

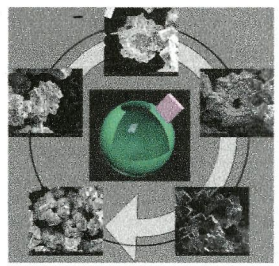

4133 S dx.doi.org/10.1021/ic3027623

Efficient Quenching of TGA-Capped CdTe Quantum Dot Emission by a Surface-Coordinated Europium(III) Cyclen Complex

Shane A. Gallagher, Steve Comby, Michal Wojdyla, Thorfinnur Gunnlaugsson, John M. Kelly, Yurii K. Gun'ko, Ian P. Clark, Gregory M. Greetham, Michael Towrie, and Susan J. Quinn*

Extremely efficient quenching of the excited state of aqueous CdTe quantum dots (QDs) by photoinduced electron transfer to a surface coordinated europium cyclen complex is elucidated using steady-state emission and picosecond transient absorption.

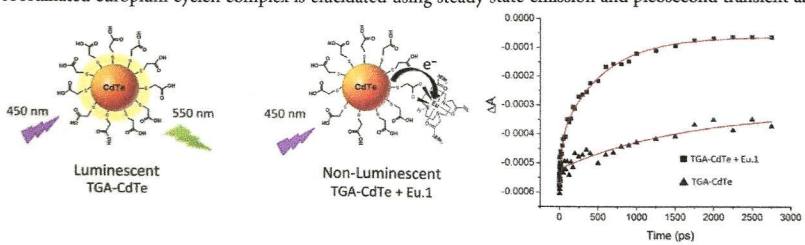

4136 S dx.doi.org/10.1021/ic4000268

Unidirectional Charge Transfer in *Di*-cobalt Valence Tautomeric Compound Finely Tuned by Ancillary Ligand

Bao Li, Li-Qin Chen, Jun Tao,* Rong-Bin Huang, and Lan-Sun Zheng

A dinuclear valence tautomeric compound containing cationic structure with crystallographically distinguishable *hs*-Co(II) and *ls*-Co(III) centers undergoes unidirectional charge transfer.

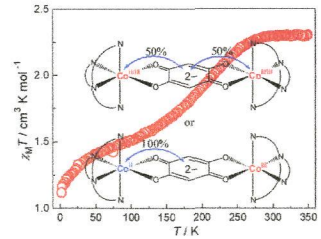

4139 S dx.doi.org/10.1021/ic400116u

Intriguing Chemistry of Molybdenum Corroles

Izana Nigel-Etinger, Israel Goldberg,* and Zeev Gross*

The development of new methodologies for gaining access to low-valent molybdenum complexes led to spectroscopic identification of mononuclear (oxo)molybdenum(IV) corroles, as well as the full characterization of a binuclear molybdenum(IV) corrole that is bridged through axial O atoms by a $Mg(THF)_4$ moiety.

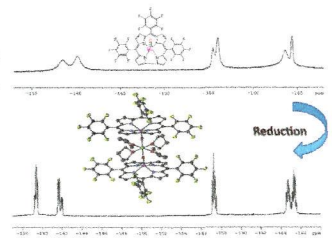

4142 S dx.doi.org/10.1021/ic4001973

Single Crystal to Single Crystal Transformation and Hydrogen-Atom Transfer upon Oxidation of a Cerium Coordination Compound

Ursula J. Williams, Brian D. Mahoney, Andrew J. Lewis, Patrick T. DeGregorio, Patrick J. Carroll, and Eric J. Schelter*

Trivalent and tetravalent cerium compounds of the octamethyltetraazaannulene (H_2omtaa) ligand have been synthesized. Electrochemical analysis shows a strong thermodynamic preference for the formal cerium(IV) oxidation state. Oxidation of the cerium(III) congener Ce(Homtaa)(omtaa) occurs by hydrogen-atom transfer that includes a single crystal to single crystal transformation upon exposure to an ambient atmosphere.

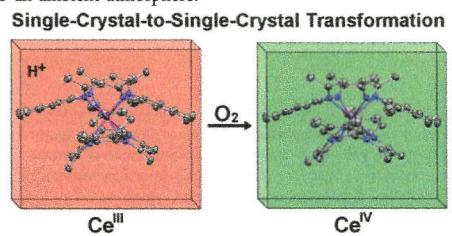

4145 S dx.doi.org/10.1021/ic400185e

Dinuclear Lanthanide(III) Complexes by Metal-Ion-Assisted Hydration of Di-2-pyridyl Ketone Azine

Nikolaos C. Anastasiadis, Carlos M. Granadeiro, Nikolaos Klouras, Luís Cunha-Silva, Catherine P. Raptopoulou, Vassilis Psycharis, Vlasoula Bekiari, Salete S. Balula,* Albert Escuer,* and Spyros P. Perlepes*

The initial employment of di-2-pyridyl ketone azine in 4f metal chemistry has led to a unique ligand transformation; the resulting anionic ligand is able to bridge two Ln^{III} ions, affording neutral and cationic dinuclear complexes with interesting properties, including single-molecule-magnetism behavior for the Dy^{III} member and catalytic activity toward styrene oxidation for the Gd^{III} compound.

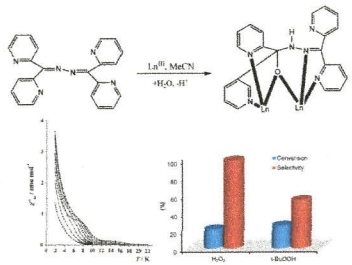

4148 S dx.doi.org/10.1021/ic4002169

Kinetically Controlling Phase Transformations of Crystalline Mercury Selenidostannates through Surfactant Media

Wei-Wei Xiong, Pei-Zhou Li, Tian-Hua Zhou, Alfred ling Yoong Tok, Rong Xu, Yanli Zhao, and Qichun Zhang*

Two novel one-dimensional mercury selenidostannates, $[DBUH]_2[Hg_2Sn_2Se_6(Se_2)]$ (**1**) and $[DBUH]_2[Hg_2Sn_2Se_7]$ (**2**), where DBU = 1,8-diazabicyclo[5.4.0]undec-7-ene, have been synthesized under surfactant-thermal conditions. Compound **1** is kinetically stable and can be transformed into thermodynamically stable phase **2** by prolonging the reaction time, while only **2** was obtained at various reaction times when the surfactant was removed under the same reaction conditions.

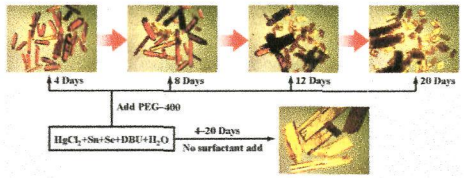

4151 S dx.doi.org/10.1021/ic400293k

Formation of $[Ni^{III}(\kappa^1\text{-}S_2CH)(P(o\text{-}C_6H_3\text{-}3\text{-}SiMe_3\text{-}2\text{-}S)_3)]^-$ via CS_2 Insertion into Nickel(III) Hydride Containing $[Ni^{III}(H)(P(o\text{-}C_6H_3\text{-}3\text{-}SiMe_3\text{-}2\text{-}S)_3)]^-$

Kuan-Ting Lai, Wei-Chieh Ho, Tzung-Wen Chiou, and Wen-Feng Liaw*

Insertion of CS_2 into the Ni^{III}–H bond of the thermally unstable $[PPN][Ni(H)(P(o\text{-}C_6H_3\text{-}3\text{-}SiMe_3\text{-}2\text{-}S)_3)]$, freshly prepared from the reaction of $[PPN][Ni(OC_6H_5)P(C_6H_3\text{-}3\text{-}SiMe_3\text{-}2\text{-}S)_3]$ and 4,4,5,5-tetramethyl-1,3,2-dioxaborolane (HBpin; pin = $OCMe_2CMe_2O$) in tetrahydrofuran at −80 °C via a metathesis reaction, readily affords $[PPN][Ni^{III}(\kappa^1\text{-}S_2CH)(P(o\text{-}C_6H_3\text{-}3\text{-}SiMe_3\text{-}2\text{-}S)_3)]$ featuring a κ^1-S_2CH moiety.

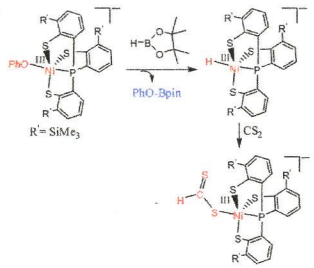

4154 S dx.doi.org/10.1021/ic4003884

Avoiding Magnetochemical Overparametrization, Exemplified by One-Dimensional Chains of Hexanuclear Iron(III) Pivalate Clusters

Svetlana G. Baca, Tim Secker, Annabel Mikosch, Manfred Speldrich, Jan van Leusen, Arkady Ellern, and Paul Kögerler*

One-dimensional chain coordination polymers based on hexanuclear iron(III) pivalate building blocks and 1,4-dioxane (diox) or 4,4′-bipyridine (4,4′-bpy) bridging ligands, $[Fe_6O_2(O_2CH_2)(O_2CCMe_3)_{12}(diox)]_n$ (**1**) and $[Fe_6O_2(O_2CH_2)(O_2CCMe_3)_{12}(4,4'\text{-bpy})]_n$ (**2**), showcase the utility of the angular overlap model, implemented in the program *wxJFinder*, in the predictive identification of the relative role of intra- and intercluster coupling.

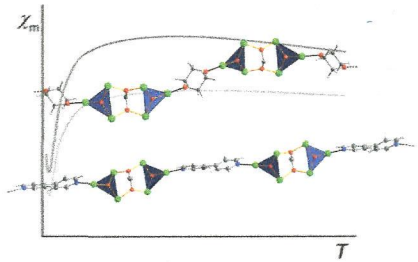

4157 S dx.doi.org/10.1021/ic4004142

Interaction of Anticancer Ruthenium Compounds with Proteins: High-Resolution X-ray Structures and Raman Microscopy Studies of the Adduct between Hen Egg White Lysozyme and AziRu

Alessandro Vergara, Gerardino D'Errico, Daniela Montesarchio, Gaetano Mangiapia, Luigi Paduano, and Antonello Merlino*

The binding properties of AziRu, a ruthenium(III) complex with high antiproliferative activity, toward a hen egg white lysozyme have been investigated by X-ray crystallography and Raman microscopy. The data provide clear evidence on the mechanism of AziRu–protein adduct formation and of ligand exchange in the crystal state.

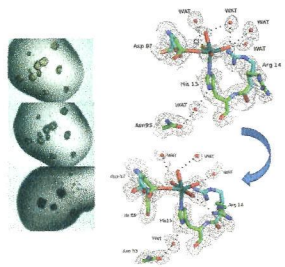

Articles

4160 S dx.doi.org/10.1021/ic300672g

Kinetics and Thermodynamics of Small Molecule Binding to Pincer-PCP Rhodium(I) Complexes

Mark D. Doherty, David C. Grills,* Kuo-Wei Huang, James T. Muckerman, Dmitry E. Polyansky,* Rudi van Eldik, and Etsuko Fujita*

The kinetics and thermodynamics of the binding of small molecules (L = N_2, H_2, D_2, and C_2H_4) to two different photogenerated, coordinatively unsaturated pincer-PCP rhodium(I) complexes have been investigated. This has revealed a mechanism in which the primary intermediate is a relatively long-lived unsolvated species. The mechanism of subsequent reactivity with L and/or solvent is determined by the structure of the PCP ligand and the nature of the solvent.

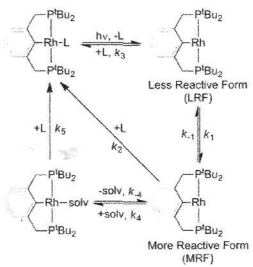

4173 Ⓢ dx.doi.org/10.1021/ic3008427

Activation of Dimanganese Class Ib Ribonucleotide Reductase by Hydrogen Peroxide: Mechanistic Insights from Density Functional Theory

Katarina Roos* and Per E. M. Siegbahn

The class Ib ribonucleotide reductase R2 subunit (R2F) utilizes a dimanganese cofactor and a flavodoxin protein to generate a tyrosyl radical, which is required for ribonucleotide reduction. An energetically feasible reaction mechanism for activation of dimanganese R2F by hydrogen peroxide is modeled using density functional theory. The reaction proceeds through two reductive half-reactions. On the basis of comparisons with the dismutation reaction in manganese catalase, a speculative role of the flavodoxin protein in radical generation is proposed.

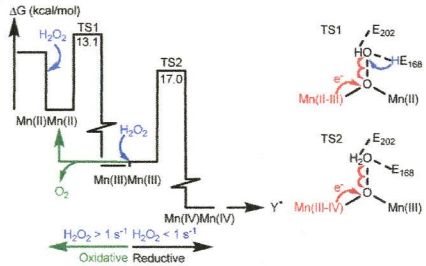

4185 Ⓢ dx.doi.org/10.1021/ic301548w

Structural and Physical Properties Diversity of New $CaCu_5$-Type Related Europium Platinum Borides

Leonid Salamakha, Ernst Bauer,* Gerfried Hilscher, Herwig Michor, Oksana Sologub, Peter Rogl,* and Gerald Giester

Three novel europium platinum borides have been synthesized by arc melting of constituent elements and subsequent annealing. They were characterized by X-ray powder and single-crystal diffraction.

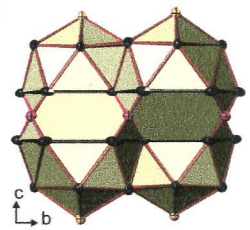

4198 Ⓢ dx.doi.org/10.1021/ic301781n

Two-Dimensional Charge-Separated Metal–Organic Framework for Hysteretic and Modulated Sorption

Sujuan Wang, Qiuli Yang, Jianyong Zhang,* Xuepeng Zhang, Cunyuan Zhao, Long Jiang, and Cheng-Yong Su*

A charge-separated metal–organic framework has been synthesized from zinc(II) dimeric secondary building unit and imidazolium tricarboxylate with an unprecedented two-dimensional 3,6-connected net with the point (Schläfli) symbol $(4^2.6)_2(4^4.6^9.8^2)$. The framework has an overall balanced charge and one-dimensional highly polar channels with positive charge located on the imidazolium/phenyl rings and negative charge on the coordinated carboxylate moieties, which results in hysteretic sorption of various gases and vapors.

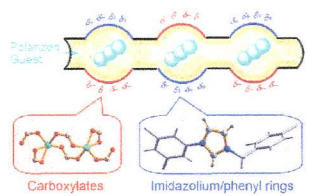

4205 Ⓢ dx.doi.org/10.1021/ic301893p

Screening Hofmann Compounds as CO_2 Sorbents: Nontraditional Synthetic Route to Over 40 Different Pore-Functionalized and Flexible Pillared Cyanonickelates

Jeffrey T. Culp,* Catherine Madden, Kristi Kauffman, Fan Shi, and Christopher Matranga

An extended series of novel functionalized dipyridyl derivatives were synthesized and intercalated between preformed polymeric cyanonickelate sheets to form a family of porous pillared Hofmann compounds which were evaluated as CO_2 sorbents. The conversion is quantitative and amenable to a wide range of functional groups. Interestingly, a number of sorbents showed structurally flexible behavior during the adsorption and desorption of CO_2.

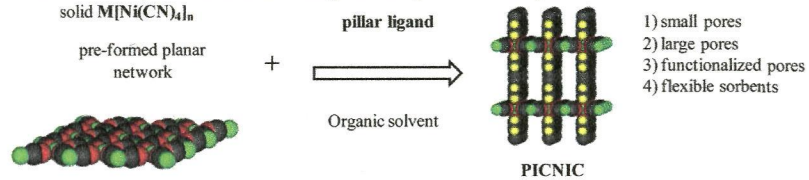

4217 Ⓢ dx.doi.org/10.1021/ic301928a

Solid-State Structure and Calculated Electronic Structure, Formation Energy, Chemical Bonding, and Optical Properties of $Zn_4O(FMA)_3$ and Its Heavier Congener $Cd_4O(FMA)_3$

Li-Ming Yang,* Ponniah Ravindran, and Mats Tilset*

The structures of $Zn_4O(FMA)_3$ and its Cd congener have been optimized by density functional theory methods. Their structures and electronic and optical properties have been analyzed and are compared to other metal–organic frameworks with IRMOF topology.

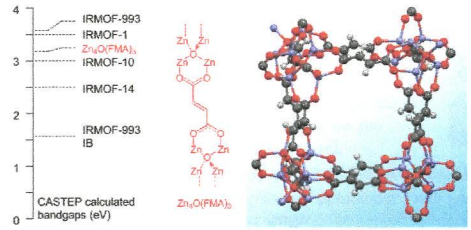

4229 Ⓢ dx.doi.org/10.1021/ic301949n

Porous Coordination Polymer Polymorphs with Different Flexible Pores Using a Structurally Flexible and Bent 1,3-Bis(4-pyridyl)propane Ligand

Katsuo Fukuhara, Shin-ichiro Noro,* Kunihisa Sugimoto, Tomoyuki Akutagawa, Kazuya Kubo, and Takayoshi Nakamura*

Two porous coordination polymer (PCP) polymorphs with the formula $[Cu(CF_3SO_3)_2(bpp)_2]_n$ [bpp = 1,3-bis(4-pyridyl)propane] showed completely different gate-opening adsorption behaviors.

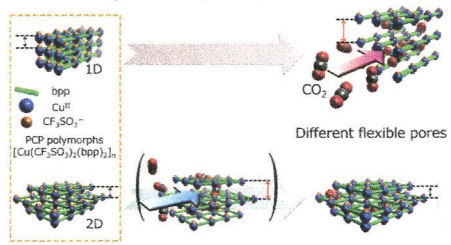

4238 Ⓢ dx.doi.org/10.1021/ic3019887

Can Molecular Cages Be Effective at Small Molecule Activation? A Computational Investigation

Nishamol Kuriakose and Kumar Vanka*

Full quantum mechanical calculations employing DFT/MP2 methods indicate that recently synthesized Ga–N cage compounds would be excellent candidates for small molecule activation, for important reactions such as the catalysis of ammonia borane dehydrogenation. Since molecular cages have never been viewed in this light, this opens up exciting new possibilities in small molecule activation research.

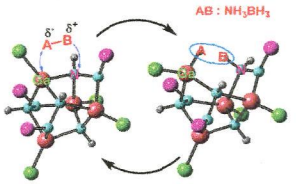

4244 Ⓢ dx.doi.org/10.1021/ic302082a

***Trans* Effect in Halobismuthates and Haloantimonates Revisited. Molecular Structures and Vibrations from Theoretical Calculations**

Hong-Li Sheu and Jaan Laane*

Ab initio and density functional theory calculations have been carried out for a series of halobismuthates and haloantimonates of formulas $MX6^{3-}$, $M_2X_9^{3-}$, and $M_2X_{10}^{4-}$ to calculate their bond distances and bond stretching frequencies. The calculations confirm and quantify the *trans* effect, which postulates that external bonds across from bridging bonds are shorter and stronger than those across from other external bonds.

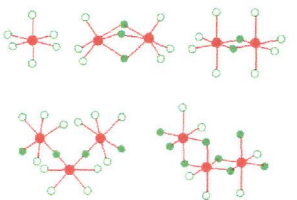

4250 Ⓢ dx.doi.org/10.1021/ic302114t

Synthesis and Structure Determination of $CaSi_{1/3}B_{2/3}O_{8/3}$: A New Calcium Borosilicate

Emmanuel Véron,* Mounesha N. Garaga, Denis Pelloquin, Sylvian Cadars, Matthew Suchomel, Emmanuelle Suard, Dominique Massiot, Valérie Montouillout, Guy Matzen, and Mathieu Allix*

This article reports on the identification, synthesis, and in-situ structure determination of a new crystalline calcium borosilicate compound, namely, $CaSi_{1/3}B_{2/3}O_{8/3}$. Synthesis was carried out by complete crystallization on annealing from a corresponding glassy composition in the widely studied $CaO–SiO_2–B_2O_3$ ternary system. The crystallographic structure was determined ab initio using electron diffraction information and the charge flipping algorithm performed on synchrotron and neutron powder diffraction data collected in situ at high temperature.

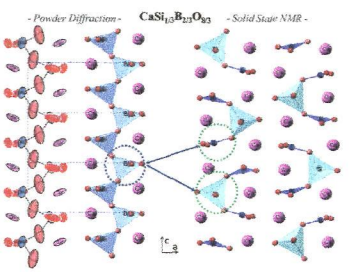

4259 Ⓢ dx.doi.org/10.1021/ic302162c

Manganese(II), Iron(II), and Mixed-Metal Metal–Organic Frameworks Based on Chains with Mixed Carboxylate and Azide Bridges: Magnetic Coupling and Slow Relaxation

Yan-Qin Wang, Qi Yue, Yan Qi, Kun Wang, Qian Sun, and En-Qing Gao*

A series of isomorphous 3D $Mn^{II}_{1-x}Fe^{II}_x$ MOFs based on a chain with $(\mu\text{-COO})_2(\mu\text{-1,1-N}_3)$ bridges shows magnetic evolution from 1D antiferromagnetism to single-chain magnets as Fe(II) gradually substitutes for Mn(II).

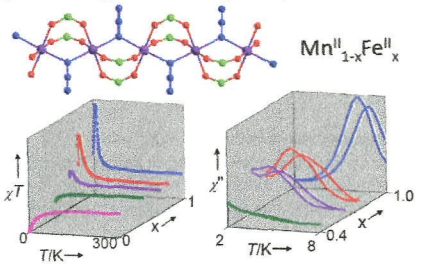

4269 Ⓢ dx.doi.org/10.1021/ic302184h

Role of Wingtip Substituents on Benzene-Platform-Based Tetrapodal Ligands toward the Formation of a Self-Assembled Silver Carbene Cage

B. Nisar Ahamed, Ranjan Dutta, and Pradyut Ghosh*

Formation of a silver-ion-assisted tetranuclear molecular box is achieved via the dimeric assembly of a tetrapodal receptor containing ethyl as the wingtip substituent. The importance of wingtips toward the formation of metallocages is demonstrated with the isolation of simple NHC-Ag complexes of *N*-methyl- and *N*-benzyl-substituted tetrapodal receptors.

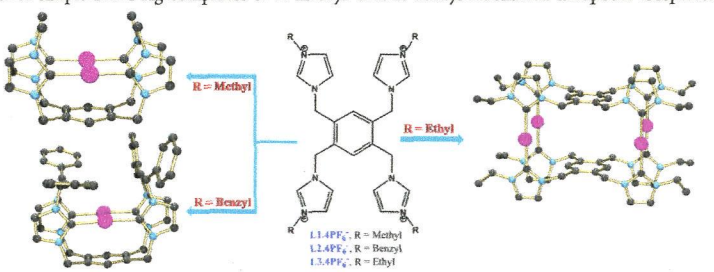

4277 S dx.doi.org/10.1021/ic302216y

Comparisons of Plutonium, Thorium, and Cerium Tellurite Sulfates

Jian Lin, Justin N. Cross, Juan Diwu, Nathan A. Meredith, and Thomas E. Albrecht-Schmitt*

$Pu(TeO_3)(SO_4)$, $Th(TeO_3)(SO_4)$, and $Ce_2(Te_2O_5)(SO_4)_2$ have been prepared hydrothermally under comparable synthetic parameters. Elucidation of the structures reveals that $Pu(TeO_3)(SO_4)$ is characterized by a neutral layer structure with no interlamellar charge-balancing ions. $Ce_2(Te_2O_5)(SO_4)_2$, however, possesses a completely different dense three-dimensional framework. Bond valence calculation and UV–vis–NIR spectra indicate that the Ce compound is trivalent whereas the Pu and Th compounds are tetravalent leading to the formation of significantly different compounds.

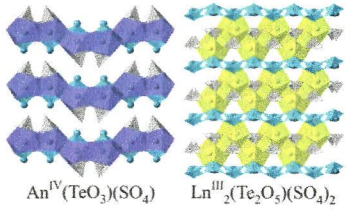

4282 S dx.doi.org/10.1021/ic3022408

Isolation, Characterization, and Nuclease Activity of Biologically Relevant Chromium(V) Complexes with Monosaccharides and Model Diols. Likely Intermediates in Chromium-Induced Cancers

Ruben Bartholomäus, Jennifer A. Irwin, Liwei Shi, Siwaporn Meejoo Smith, Aviva Levina, and Peter A. Lay*

The first isolation and characterization of Cr(V) complexes with monosaccharide ligands ($[Cr^{V}OL_2]^-$, where LH_2 = d-glucose, d-mannose, d-galactose, or d-ribose) have been reported. Such complexes are postulated as likely intermediates both in Cr(VI)-induced carcinogenicity and in antidiabetic activity of Cr(III). The ability of chromium(V) monosaccharide complexes to cause oxidative DNA damage in the absence of added oxidants or reductants has been definitively established for the first time.

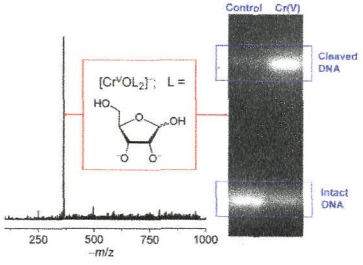

4293 S dx.doi.org/10.1021/ic302264t

1,3-Dipolar Cycloadditions of Ruthenium(II) Azido Complexes with Alkynes and Nitriles

S. Miguel-Fernández, S. Martínez de Salinas, J. Díez, M. P. Gamasa, and E. Lastra*

The diazido complex $[Na][Ru(N_3)_2\{\kappa^3(N,N,N)\text{-Tpms}\}(PPh_3)]$ reacts with alkynes and nitriles. The reaction with fumaronitrile leads to a complex containing a new $\kappa^2(N^1,N^3)$-5-(1,2,3-triazol-4-yl)-1,2,3,4-tetrazolate ligand obtained through two consecutive cycloaddition reactions. The structure of the resulting complex has been determined by X-ray diffraction, and the mechanism for this transformation has been unambiguously established.

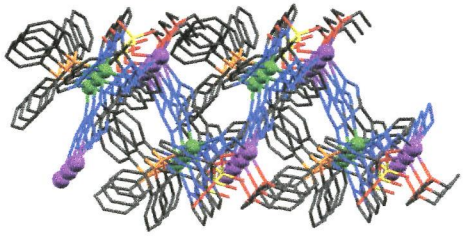

4303 S dx.doi.org/10.1021/ic302289r

Mixed Ligand Cu^{2+} Complexes of a Model Therapeutic with Alzheimer's Amyloid-β Peptide and Monoamine Neurotransmitters

Vijaya B. Kenche, Izabela Zawisza, Colin L. Masters, Wojciech Bal, Kevin J. Barnham, and Simon C. Drew*

Ternary metal complexes of 2-substituted 8-hydroxyquinolines have numerous proposed biological applications, including use as medical imaging agents, enzyme inhibitors, an artificial nucleobase and as metal chaperones. In this study, we demonstrate that 2-[(dimethylamino)methyl]-8-hydroxyquinoline forms ternary Cu^{2+} complexes with histidine side chains of proteins and peptides including Aβ, and with monoamine neurotransmitters. We discuss the significance of these findings in the context of therapeutic applications to neurodegenerative diseases.

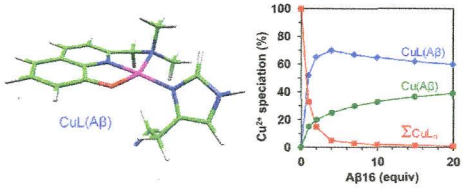

4319 S dx.doi.org/10.1021/ic302323j

$[Li(XeF_2)_n](AF_6)$ (A = P, As, Ru, Ir), the First Xenon(II) Compounds of Lithium. Synthesis, Raman Spectrum, and Crystal Structure of $[Li(XeF_2)_3](AsF_6)$

Gašper Tavčar* and Boris Žemva

$[Li(XeF_2)_3](AsF_6)$ is the first compound that has been structurally characterized in which XeF_2 is coordinated to an alkali-metal center. In addition, it has been shown by Raman spectroscopy that coordination of XeF_2 also occurred in the cases of $LiAF_6$ (A = P, As, Ru, Ir), whereas in the cases of A = V, Sb, Nb, Ta, and XeF_2, coordination was not observed.

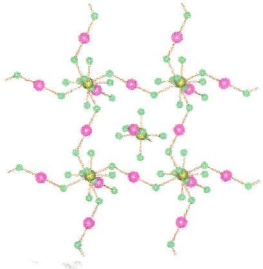

4324 Ⓢ dx.doi.org/10.1021/ic302352k

Integration of Alkyl-Substituted Bipyridyl Benzenedithiolato Platinum(II) Complexes with Cadmium(II) Ion via Selective Dative Bond Formation

Hirotaka Honda, Takeshi Matsumoto, Misaki Sakamoto, Atsushi Kobayashi, Ho-Chol Chang,* and Masako Kato

Platinum complexes, [Pt(1,2-benzenedithiolato)(4,4′-di-*tert*-butyl-2,2′-bipyridine)] and [Pt(1,2-benzenedithiolato)(4,4′-ditridecyl-2,2′-bipyridine)], bind selectively with Cd(II) by forming dative bonds to give a twisted trinuclear complex, $[Cd\{Pt(Bdt)(DTBbpy)\}_2(ClO_4)(H_2O)](ClO_4)$, and a shuttlecock-shaped tetranuclear complex, $[Cd\{Pt(Bdt)(C13bpy)\}_3(H_2O)](ClO_4)_2\cdot CH_2Cl_2$, respectively, depending upon the alkyl groups substituted on the bpy moieties.

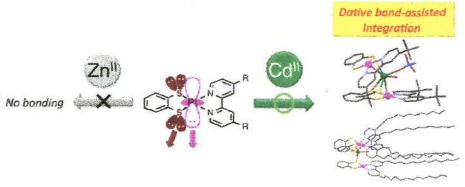

4335 Ⓢ dx.doi.org/10.1021/ic302481s

New Dinuclear Ruthenium Complexes: Structure and Oxidative Catalysis

Carlo Di Giovanni, Lydia Vaquer, Xavier Sala, Jordi Benet-Buchholz, and Antoni Llobet*

New dinuclear ruthenium complexes have been prepared and spectroscopically and electrochemically characterized. Their corresponding Ru-aqua complex is a powerful catalyst for the stereoselective epoxidation of alkenes to epoxides. New dinuclear ruthenium complexes catalyze efficiently the epoxidation of alkenes.

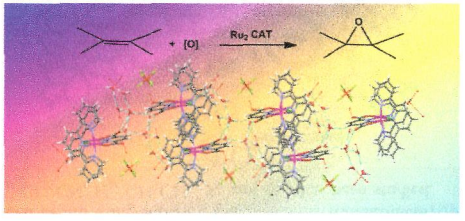

4346 Ⓢ dx.doi.org/10.1021/ic3024875

Synthetic, Structural, NMR, and Computational Study of a Geminally Bis(*peri*-substituted) Tridentate Phosphine and Its Chalcogenides and Transition-Metal Complexes

Matthew J. Ray, Rebecca A. M. Randall, Kasun S. Athukorala Arachchige, Alexandra M. Z. Slawin, Michael Bühl, Tomas Lebl, and Petr Kilian*

Coupling of two acenaphthene backbones through a phosphorus atom gives the first geminally bis(*peri*-substituted) tridentate phosphine. Contrary to our expectations, this tridentate phosphine accommodates a surprisingly wide range of bonding geometries in both chalcogenides and transition-metal complexes.

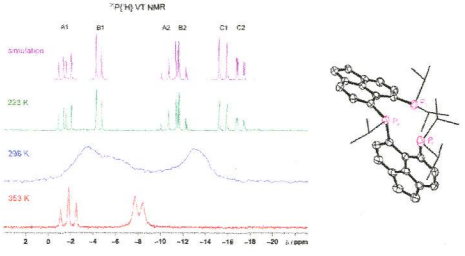

4360 Ⓢ dx.doi.org/10.1021/ic3024919

l-Tyrosinatonickel(II) Complex: Synthesis and Structural, Spectroscopic, Magnetic, and Biological Properties of $2\{[Ni(l\text{-}Tyr)_2(bpy)]\}\cdot 3H_2O\cdot CH_3OH$

Agnieszka Wojciechowska,* Anna Gągor, Marek Duczmal, Zbigniew Staszak, and Andrzej Ozarowski

This work presents the synthesis and structural and spectroscopic (FT-IR, NIR–vis–UV, and HFEPR) characterization of a new l-tyrosinato six-coordinated Ni^{2+} ion complex, $2\{[Ni(l\text{-}Tyr)_2(bpy)]\}\cdot 3H_2O\cdot CH_3OH$ (**1**). The obtained experimental set of spectroscopic parameters *B*, *C*, *Dq*, *Ds*, *Dt*, *D*, *E*, and g_{av} gives well agreement with magnetic studies. Complex **1** was also tested for antifungal and antibacterial properties.

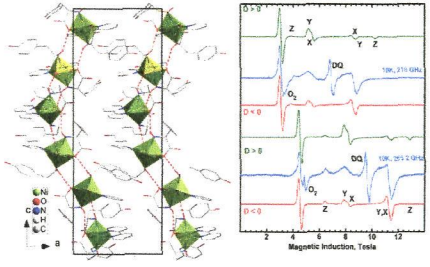

4372 Ⓢ dx.doi.org/10.1021/ic302494a

Trace Level Uranyl Complexation with Phenylphosphonic Acid in Aqueous Solution: Direct Speciation by High Resolution Mass Spectrometry

Catherine Galindo* and Mirella Del Nero

Orbitrap mass spectrometry was successfully used to investigate the complexation of uranyl at trace level by phenylphosphonic acid. Direct analysis of the native solutions (without adding any cosolvent) revealed the coexistence of three U(VI)-phenylphosphonate complexes at pH 3. A strategy based on the use of uranyl-phosphate solution complexes as internal standards was developed to determine from the ESI(-)MS results the stability constants of the U(VI)-phenylphosphonate complexes.

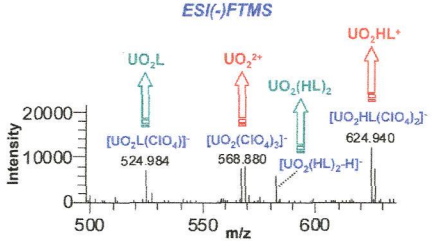

4384 Ⓢ dx.doi.org/10.1021/ic3025414

PPh_3-Derivatives of $[Pt_{3n}(CO)_{6n}]^{2-}$ (n = 2–6) Chini's Clusters: Syntheses, Structures, and ^{31}P NMR Studies

Iacopo Ciabatti, Cristina Femoni, Maria Carmela Iapalucci, Giuliano Longoni, Tatiana Lovato, and Stefano Zacchini*

The stepwise substitution of CO with PPh_3 in $[Pt_{3n}(CO)_{6n}]^{2-}$ has been studied by FT-IR, $^{31}P\{^1H\}$ NMR spectroscopy, ESI-MS, and X-ray crystallography, disclosing several PPh_3-derivatives of the Chini's clusters.

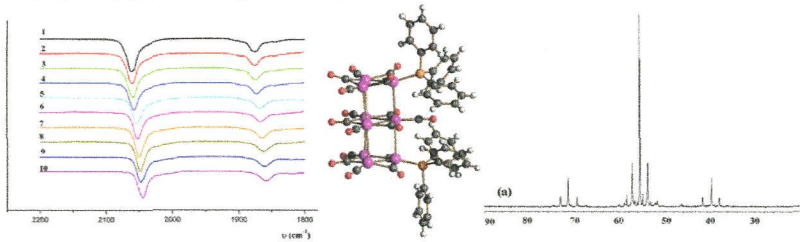

4396 Ⓢ dx.doi.org/10.1021/ic302553z

Picolyl–NHC Hydrotris(pyrazolyl)borate Ruthenium(II) Complexes: Synthesis, Characterization, and Reactivity with Small Molecules

Francys E. Fernández, M. Carmen Puerta,* and Pedro Valerga*

Hydrotris(pyrazolyl)borate ruthenium(II) complexes with picolyl functionalyzed N-heterocyclic carbenes $[(\kappa^3\text{-Tp})Ru(L)(Cl)]$ (L = picolylimidazol-2-ylidene ligands) have been synthesized and characterized. The reactivity of the 16-electron species, $[(\kappa^3\text{-Tp})Ru(L)]^+$, generated in situ using $NaBAr^F_4$ (Ar^F = 3,5-bis(trifluoromethyl)phenyl) as a halide scavenger, toward small molecules (CO, N_2, CH_3CN, H_2, CH_2CH_2, S_8, and O_2) has been studied.

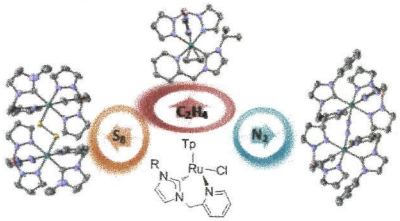

4411 Ⓢ dx.doi.org/10.1021/ic302593f

Phase Progression of γ-Al_2O_3 Nanoparticles Synthesized in a Solvent-Deficient Environment

Stacey J. Smith, Samrat Amin, Brian F. Woodfield, Juliana Boerio-Goates, and Branton J. Campbell*

The phase-progression of Al_2O_3 nanoparticles synthesized from a novel solvent-deficient method, indicating that γ-Al_2O_3 (green triangles) is present at 300°C but is riddled with boehmite-like stacking-fault defects (blue circles) that heal steadily between 300–950°C prior to an abrupt transformation to α-Al_2O_3 (red squares) at ~1050°C.

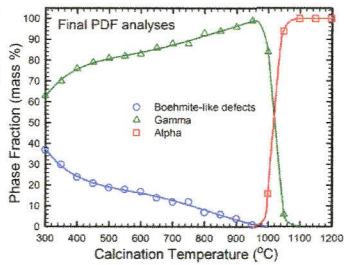

4424 Ⓢ dx.doi.org/10.1021/ic302613g

Synthesis of Complex Polymeric Telluridoindates from $KInTe_2$

Johanna Heine, Silke Santner, and Stefanie Dehnen*

$KInTe_2$ was used as starting material for the preparation of four new polymeric telluridoindate phases with complex cations, using different synthetic approaches. All title compounds are based on $[InTe_4]$ tetrahedra as the primary building unit, however, with significant increase in complexity in going from simple chain-like anionic structures in $[K(18\text{-crown-}6)][InTe_2]\cdot 2en$ (**1**) and $[K([2.2.2]crypt)]_2[In_2Te_6]\cdot 0.5en$ (**2**) to an intricate band-type anion in $[HTMDP]_2[In_4Te_8]$ (**3**), and finally an anionic framework with **lig**-topology in $[HDAP]_8[In_{12}Te_{23}]$ (**4**).

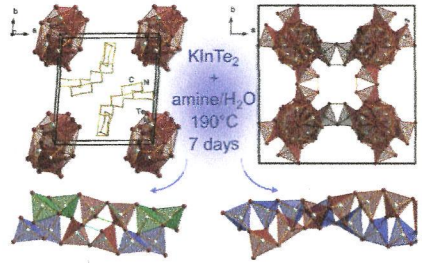

4431 Ⓢ dx.doi.org/10.1021/ic302643w

Synthesis, Crystal Structure, and Solid-State NMR Investigations of Heteronuclear Zn/Co Coordination Networks — A Comparative Study

Anusree Viswanath Kuttatheyil, Daniel Lässig, Jörg Lincke, Merten Kobalz, Maria Baias, Katja König, Jörg Hofmann, Harald Krautscheid, Chris J. Pickard, Jürgen Haase, and Marko Bertmer*

Synthesis and solid-state NMR characterization of two isomorphous series of zinc and cobalt coordination networks with 1,2,4-triazolyl benzoate ligands are reported. Both series consist of 3D diamondoid networks with four-fold interpenetration. Solid-state NMR identifies the metal coordination of the ligands, and assignment of all ^1H and ^{13}C shifts was enabled by the combination of ^{13}C editing and FSLG-HETCOR spectra, and 2D ^1H–^1H back-to-back (BABA) spectra with results from NMR-CASTEP calculations.

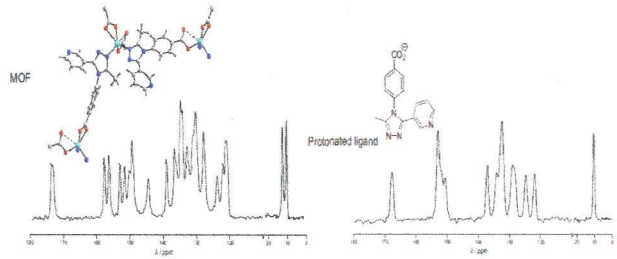

4443 dx.doi.org/10.1021/ic302649s

Crystal Chemistry, Band Engineering, and Photocatalytic Activity of the $LiNb_3O_8$–$CuNb_3O_8$ Solid Solution

Prangya Parimita Sahoo and Paul A. Maggard*

A continuous solid solution $Li_{1-x}Cu_xNb_3O_8$ ($0 \le x \le 1$) has been isolated in the phase diagram of Li_2O–Cu_2O–Nb_2O_5. The band gap decreases sharply with the increase in Cu(I) content in the system. While $LiNb_3O_8$ is a UV-active photocatalyst, the substitution of Cu(I) into the structure yields visible-light photocatalytic activity.

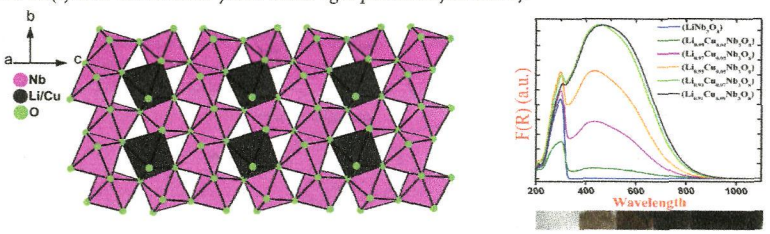

4451 dx.doi.org/10.1021/ic3026914

Soluble Molybdenum(V) Imido Phthalocyanines and Pyrazinoporphyrazines: Crystal Structure, UV–vis and Electron Paramagnetic Resonance Spectroscopic Studies

Elisabeth Seikel, Benjamin Oelkers, Olaf Burghaus, and Jörg Sundermeyer*

Soluble imido phthalocyanines [Pc#Mo(NR)Cl] and pyrazinoporphyrazines [Ppz#Mo(NR)Cl] (R = *t*Bu, Mes) were prepared and studied by XRD analysis, UV–vis and EPR spectroscopy. Unexpected differences between alkyl and aryl imido complexes indicate different electronic structures.

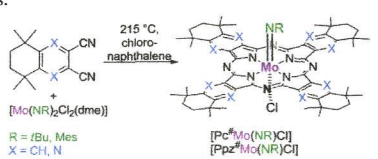

4458 dx.doi.org/10.1021/ic3027094

Diffusion-Controlled Formation of Ti_2O_3 during Spark-Plasma Synthesis

I. Veremchuk,* I. Antonyshyn, C. Candolfi, X. Feng, U. Burkhardt, M. Baitinger, J.-T. Zhao, and Yu. Grin

The spark-plasma-sintering technique has been successfully applied for the single-step direct synthesis of Ti_2O_3 from a mixture of powders of rutile/anatase with titanium.

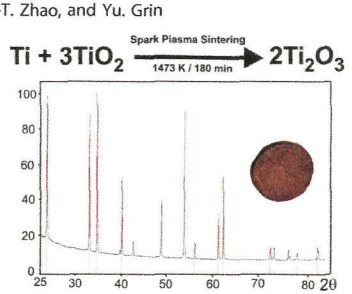

4464 dx.doi.org/10.1021/ic3027418

Highly Reduced Double-Decker Single-Molecule Magnets Exhibiting Slow Magnetic Relaxation

Mathieu Gonidec, Itana Krivokapic, Jose Vidal-Gancedo, E. Stephen Davies, Jonathan McMaster, Sergiu M. Gorun,* and Jaume Veciana*

The first halogenated phthalocyanine double-decker lanthanide complex, $F_{64}Pc_2Tb$ ($\mathbf{1}_{Tb}$), exhibits single-molecule magnet properties in its three stable reduced states, $\mathbf{1}_{Tb}^{-}$, $\mathbf{1}_{Tb}^{-2\bullet}$, and $\mathbf{1}_{Tb}^{-3}$.

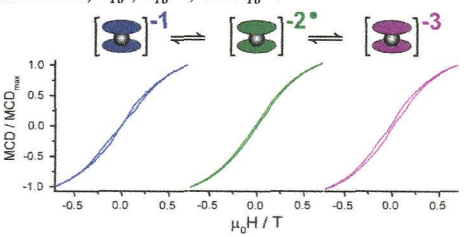

4472 dx.doi.org/10.1021/ic302743s

New Complexes of Chromium(III) Containing Organic π-Radical Ligands: An Experimental and Density Functional Theory Study

Mei Wang, Jason England, Thomas Weyhermüller, Swarna-Latha Kokatam, Christopher J. Pollock, Serena DeBeer, Jingmei Shen, Glenn P.A. Yap, Klaus H. Theopold, and Karl Wieghardt*

The electronic structures of several chromium complexes of varying formal oxidation state were investigated using a range of spectroscopic techniques, including X-ray absorption spectroscopy (XAS), X-ray crystallography, SQUID, electrochemistry, and electronic spectroscopy. These studies were supplemented by density functional theory (DFT) calculations and allowed unambiguous assignment of the true oxidation state of the chromium center. The resulting picture is remarkably uniform and serves to highlight the ubiquitous nature of ligand redox noninnocence.

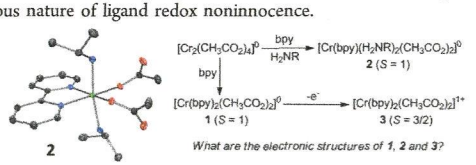

4488 dx.doi.org/10.1021/ic302759k

Facile One-Step Synthesis of MPHMes from $MesPCl_2$ (M = Li, Na, K; Mes = 2,4,6-$Me_3C_6H_2$)

Ivana Jevtovikj, Rebeca Herrero, Santiago Gómez-Ruiz, Peter Lönnecke, and Evamarie Hey-Hawkins*

Reaction of alkali metals (Li, Na, K) with mesityldichlorophosphane ($MesPCl_2$, Mes = 2,4,6-$Me_3C_6H_2$) in ethereal solvents leads to the corresponding mesitylphosphanides MPHMes in good purity and yield. ^{31}P NMR spectroscopic studies in deuterated solvents strongly support a mechanism of the reaction that involves protonation/disproportionation steps in which the solvent is the only possible proton source.

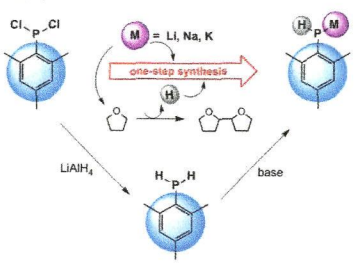

4494 Ⓢ dx.doi.org/10.1021/ic302764k

Synthesis and Size Control of Iron(II) Hexacyanochromate(III) Nanoparticles and the Effect of Particle Size on Linkage Isomerism

Matthieu F. Dumont, Olivia N. Risset, Elisabeth S. Knowles, Takashi Yamamoto, Daniel M. Pajerowski, Mark W. Meisel,* and Daniel R. Talham*

Highly reproducible, monodisperse cubic-shaped iron hexacyanochromate nanocrystals were synthesized. A kinetic study of the linkage isomerism at different temperatures shows the evolution of E_a with the size of the particles, the rate of isomerization being inversely proportional to the particle size. Using the measured thermodynamic properties and a simple two-component structural constraint hypothesis, differences in E_a for surface processes vs bulk processes were estimated.

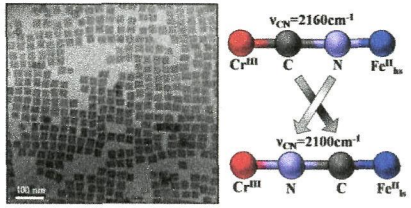

4502 Ⓢ dx.doi.org/10.1021/ic302776d

Structures of, and Related Consequences of Deprotonation on, Two C_s-Symmetric *Arachno* Nine-Vertex Heteroboranes, 4,6-$X_2B_7H_9$ (X = CH_2; S) Studied by Gas Electron Diffraction/Quantum Chemical Calculations and GIAO/NMR

Derek A. Wann,* Paul D. Lane, Heather E. Robertson, Josef Holub, and Drahomír Hnyk*

The structures of *arachno*-4,6-$(CH_2)_2B_7H_9$ and *arachno*-4,6-$S_2B_7H_9$ have been determined by combining quantum-chemical calculations and gas electron diffraction data. GIAO-MP2 methods have been used to compare ^{11}B NMR chemical shifts for various experimental and calculated geometries.

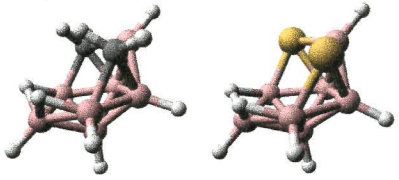

4509 Ⓢ dx.doi.org/10.1021/ic302804d

Dehydrocoupling of Dimethylamine Borane Catalyzed by $Rh(PCy_3)_2H_2Cl$

Laura J. Sewell, Miguel A. Huertos, Molly E. Dickinson, Andrew S. Weller,* and Guy C. Lloyd-Jones

The mechanism by which the neutral catalyst $Rh(PCy_3)H_2Cl$ mediates the dehydrogenation of $H_3B{\cdot}NMe_2H$ to ultimately afford the dimeric aminoborane $[H_2B{=}NMe_2]$ has been probed by stoichiometric, catalytic, and kinetic studies.

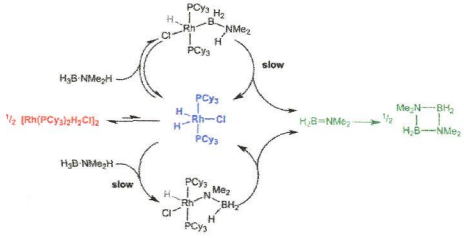

4517 Ⓢ dx.doi.org/10.1021/ic302819j

***cis*-1,3,5-Triaminocyclohexane as a Facially Capping Ligand for Ruthenium(II)**

Aimee J. Gamble, Jason M. Lynam,* Robert J. Thatcher, Paul H. Walton,* and Adrian C. Whitwood

A series of ruthenium(II) complexes containing *cis*-1,3,5-triaminocyclohexane (tach) as a facially capping ligand is reported. An analysis of the structural metrics of these compounds indicates that within this series of compounds tach is acting as a hard donor ligand which influences the nature of the coligands which are preferred in the coordination environment of the metal. Furthermore the N−H groups from tach are shown to engage in both intra- and intermolecular hydrogen bonding.

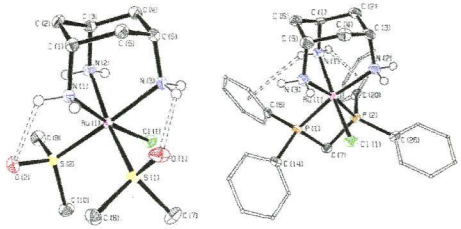

4528 Ⓢ dx.doi.org/10.1021/ic302834e

Platinum-Mediated Dinitrogen Liberation from 2-Picolyl Azide through a Putative Pt=N Double Bond Containing Intermediate

Balazs Pinter, Damijana Urankar, Andrej Pevec, Frank De Proft,* and Janez Košmrlj*

2-Picolyl azide is shown to react with *cis*-$[PtCl_2(DMSO)_2]$ to allow the formation of the diimino complex $[PtCl_2\{NH{=}C(H)Py\}]$ with subsequent dinitrogen liberation. This transformation involves a highly reactive intermediate with a Pt=N double bond formed after the extrusion of N_2 from the azide functionality.

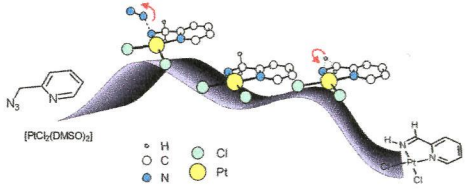

4534 Ⓢ dx.doi.org/10.1021/ic400024r

Oxorhenium Complexes Bearing the Water-Soluble Tris(pyrazol-1-yl)methanesulfonate, 1,3,5-Triaza-7-phosphaadamantane, or Related Ligands, as Catalysts for Baeyer−Villiger Oxidation of Ketones

Luísa M. D. R. S. Martins,* Elisabete C. B. A. Alegria, Piotr Smoleński, Maxim L. Kuznetsov, and Armando J. L. Pombeiro*

New water-soluble rhenium(VII or III) complexes have been prepared and shown to exhibit high activity and selectivity as catalyst precursors for the Baeyer−Villiger oxidation with H_2O_2 of cyclic and linear ketones to the corresponding lactones or esters.

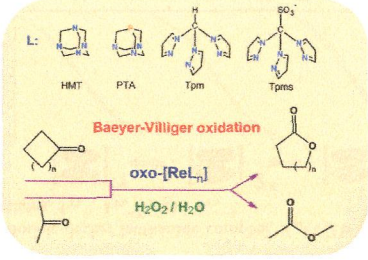

4547 S dx.doi.org/10.1021/ic400068y

Influence of the Metal (Al, Cr, and Co) and Substituents of the Porphyrin in Controlling Reactions Involved in Copolymerization of Propylene Oxide and Carbon Dioxide by Porphyrin Metal(III) Complexes. 3. Cobalt Chemistry

Chandrani Chatterjee, Malcolm H. Chisholm,* Adnan El-Khaldy, Ruaraidh D. McIntosh, Jeffrey T. Miller, and Tianpin Wu

A series of cobalt(III) complexes LCoX, where L = 5,10,15,20-tetraphenylporphyrin (TPP), 5,10,15,20-tetrakis-(pentafluorophenyl)porphyrin (TFPP), and 2,3,7,8,12,13,17,18-octaethylporphyirn (OEP) and X = Cl or acetate, has been investigated for homopolymerization of propylene oxide (PO) and copolymerization of PO and CO_2 to yield polypropylene oxide (PPO) and polypropylene carbonate (PPC) or propylene carbonate (PC), respectively. These reactions were carried out both with and without the presence of a cocatalyst, namely, 4-dimethylaminopyridine (DMAP) or PPN^+Cl^- (bis(triphenylphosphine)iminium chloride).

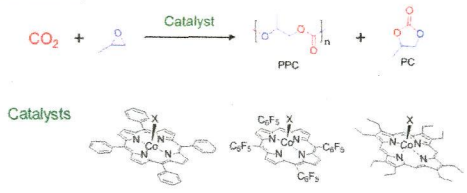

4554 S dx.doi.org/10.1021/ic400073y

Slow Magnetic Relaxation in Co(III)–Co(II) Mixed-Valence Dinuclear Complexes with a $Co^{II}O_5X$ (X = Cl, Br, NO_3) Distorted-Octahedral Coordination Sphere

Vadapalli Chandrasekhar,* Atanu Dey, Antonio J. Mota, and Enrique Colacio*

The reaction of the multisite coordination ligand (LH_4) with $CoX_2 \cdot nH_2O$ in the presence of tetrabutylammonium hydroxide affords a series of homometallic dinuclear mixed-valence complexes, $[Co^{III}Co^{II}(LH_2)_2(X)(H_2O)](H_2O)_m$ (**1**, X = Cl and m = 4; **2**, X = Br and m = 4; **3**, X = NO_3 and m = 3).

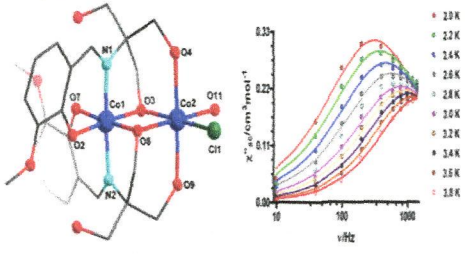

4562 S dx.doi.org/10.1021/ic400091j

Octanuclear {Ln(III)$_8$}(Ln = Gd, Tb, Dy, Ho) Macrocyclic Complexes in a Cyclooctadiene-like Conformation: Manifestation of Slow Relaxation of Magnetization in the Dy(III) Derivative

Vadapalli Chandrasekhar,* Prasenjit Bag, and Enrique Colacio

The reaction of a multidentate coordinating Schiff base ligand (LH_5) with Lanthanide(III) nitrate salts in presence of triethylamine as base, afforded a series of macrocyclic octanuclear lanthanide complexes $[Ln_8(LH_2)_4(\mu\text{-Piv})_4(\eta^2\text{-Piv})_4(\mu\text{-OMe})_4]$ {Ln = Gd(**1**), Tb(**2**), Dy(**1**), Ho(**4**)}. In these the metals are distributed over 8 vertices of an octagon, resembling an *cyclooctadiene-type* conformation. The details of magnetochemical analysis for all the complexes revealed the presence of slow relaxation of magnetization in the Dy(III) derivative.

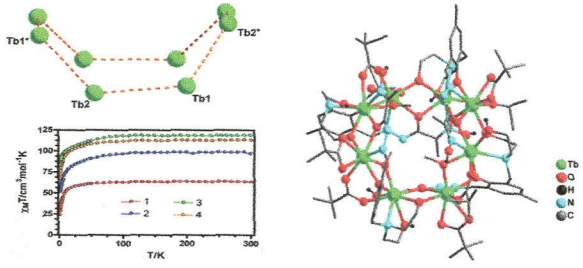

4571 S dx.doi.org/10.1021/ic400056f

Synthesis of Hetero-Binuclear Complexes from Bisgermavinylidene

Wing-Por Leung,* Kwok-Wai Kan, Yuk-Chi Chan, and Thomas C. W. Mak

Bisgermavinylidene $[(Me_3SiN{=}PPh_2)_2C{=}Ge{\rightarrow}Ge{=}C(PPh_2{=}NSiMe_3)_2]$ (**1**) has been used as the source of unstable germavinylidene for the synthesis of a series of hetero-binuclear complexes. The results suggested that germanium–carbon bonding in germavinylidene is capable of forming addition reaction products. The X-ray structures of **2**–**6** have been determined.

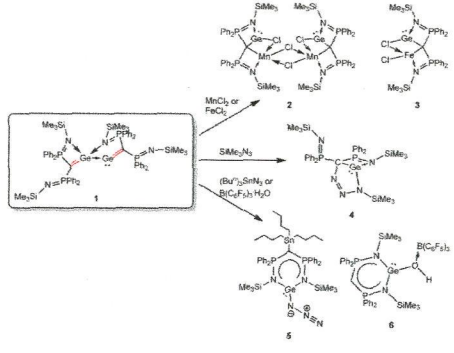

4578 Ⓢ dx.doi.org/10.1021/ic4001158

Electron Paramagnetic Resonance Analysis of a Transient Species Formed During Water Oxidation Catalyzed by the Complex Ion $[(bpy)_2Ru(OH_2)]_2O^{4+}$

Jamie A. Stull, Troy A. Stich, James K. Hurst, and R. David Britt*

In the present work, the electronic and geometric structures of the ruthenium "blue dimer" $[(bpy)_2Ru(OH_2)]_2O^{4+}$ were explored using a variety of EPR techniques. Our studies strongly suggest that the accumulating transient is an $S = 1/2$ species. This spin state is consistent with a limited number of electronic structures, each of which is discussed. Notably, the observed large metal hyperfine coupling indicates that the orbital carrying the unpaired spin has significant ruthenium character.

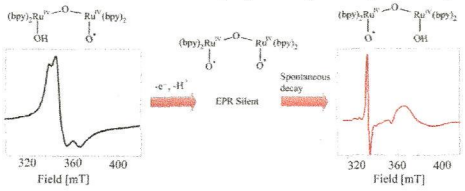

4587 Ⓢ dx.doi.org/10.1021/ic400150f

Modulating Magnetic Dynamics of Dy_2 System through the Coordination Geometry and Magnetic Interaction

Peng Zhang, Li Zhang, Shuang-Yan Lin, Shufang Xue, and Jinkui Tang*

Two Dy_2 compounds show distinct magnetic properties, highlighting the significant role played by coordination geometry and magnetic interaction in modulating the relaxation dynamics of SMMs.

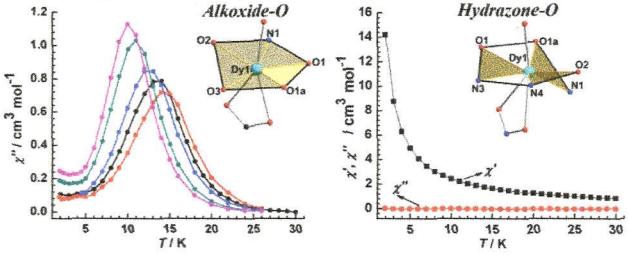

4593 Ⓢ dx.doi.org/10.1021/ic400192c

Silver(I) Complex Formation with Cysteine, Penicillamine, and Glutathione

Bonnie O. Leung, Farideh Jalilehvand,* Vicky Mah, Masood Parvez, and Qiao Wu

Silver(I) complexes with glutathione and penicillamine (H_2Pen) in alkaline aqueous solution predominantly have digonal AgS_2 coordination, with mean Ag−S bond distances from EXAFS of 2.36 ± 0.02 and 2.40 ± 0.02 Å, respectively. With cysteine oligomeric AgS_3 coordinated complexes with a mean Ag−S bond distance of 2.47 ± 0.02 Å occur, supported by ^{109}Ag NMR spectra. The $Ag(HPen)\cdot H_2O$ compound contains intertwined polymeric −Ag−S(R)−Ag−S-(R)− double strands with near-linear AgS_2 coordination, while the silver(I)−cysteinato compound $(NH_4)Ag_2(HCys)Ag(Cys)\cdot H_2O$ contains layers with connected AgS_3 and AgS_3N coordination sites.

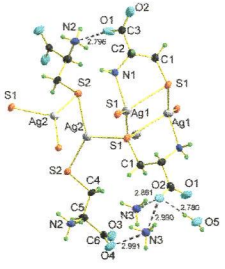

4603 Ⓢ dx.doi.org/10.1021/ic400198g

Synthesis and Characterization of Low-Generation Polyamidoamine (PAMAM) Dendrimer−Sodium Montmorillonite (Na-MMT) Clay Nanocomposites

Amila U. Liyanage, Esther U. Ikhuoria, Adeniyi A. Adenuga, Vincent T. Remcho, and Michael M. Lerner*

Lower generation (G0.0−G2.0) polyamidoamine (PAMAM) dendrimer/sodium montmorillonite (Na-MMT) nanocomposites were prepared using a solution-phase exfoliation/adsorption reaction. In the nanocomposites, PAMAM dendrimers form highly flattened monolayers or bilayers.

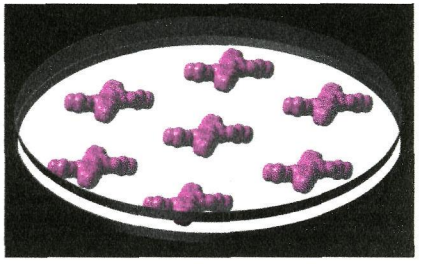

4611 Ⓢ dx.doi.org/10.1021/ic400240b

Iridium Porphyrins in CD_3OD: Reduction of Ir(III), CD_3−OD Bond Cleavage, Ir−D Acid Dissociation and Alkene Reactions

Salome Bhagan, Gregory H. Imler, and Bradford B. Wayland*

Iridium(III) tetra(*p*-sulfonatophenyl)porphyrin $[(TSPP)Ir^{III}]$ forms an equilibrium distribution of methanol and methoxide complexes. Reaction of $[(TSPP)Ir^{III}$ with dihydrogen (D_2) in methanol produces an iridium hydride $[(TSPP)Ir^{III}-D-(CD_3OD)]^{4-}$ with an acid dissociation constant (298 K) of 3.5×10^{-12}. The iridium(I) complex ($[(TSPP)Ir^{I}(CD_3OD)]^{5-}$) catalyzes reaction of $[(TSPP)Ir^{III}-D(CD_3OD)]^{4-}$ with CD_3−OD to produce an iridium methyl complex $[(TSPP)-Ir^{III}-CD_3(CD_3OD)]^{4-}$ and D_2O. Equilibrium constants are reported for reactions of the iridium(III) complexes with hydrogen and the iridium hydride with alkenes.

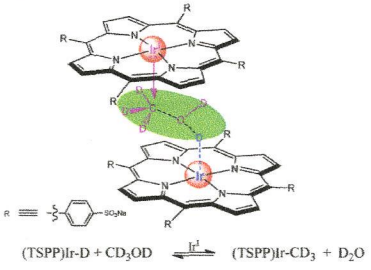

4618 Ⓢ dx.doi.org/10.1021/ic400248m

Hydrothermal Synthesis, Crystal Structure, and Catalytic Potential of a One-Dimensional Molybdenum Oxide/Bipyridinedicarboxylate Hybrid

Tatiana R. Amarante, Patrícia Neves, Anabela A. Valente, Filipe A. Almeida Paz,* Andrew N. Fitch, Martyn Pillinger, and Isabel S. Gonçalves

The reaction of MoO_3, 2,2′-bipyridine-5,5-dicarboxylic acid (H_2bpdc), water, and dimethylformamide at 150 °C leads to the isolation of the molybdenum oxide/bipyridinedicarboxylate hybrid material (DMA)[MoO_3(Hbpdc)]·nH_2O (**1**) (DMA = dimethylammonium). The structure of **1** was solved and refined through Rietveld analysis of high resolution synchrotron X-ray powder diffraction data in conjunction with information obtained from other techniques. The catalytic potential of **1** was investigated in the epoxidation reactions of the bioderived olefins methyl oleate and dl-limonene.

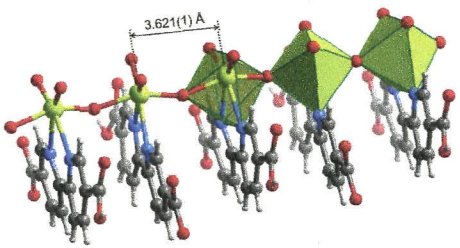

4629 dx.doi.org/10.1021/ic400250n

Pressure-Dependent Reversible Increase in T_c for the Ferrimagnetic 2-D Mn^{II}(TCNE)I(OH_2) and 3-D $Mn^{II}(TCNE)_{3/2}(I_3)_{1/2}$·zTHF Organic-Based Magnets

Jack G. DaSilva, Amber C. McConnell, and Joel S. Miller*

The pressure dependence of the magnetic properties of ferrimagnetic Mn^{II}(TCNE)I(OH_2) up to 14.05 kbar and $Mn^{II}(TCNE)_{3/2}(I_3)_{1/2}$·zTHF up to 14.32 kbar was studied. For Mn^{II}(TCNE)I(OH_2), two distinct pressure regions separated by ~1 kbar were evident in both the temperature and the field-dependent magnetic measurements.

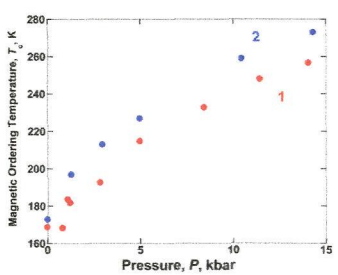

4635 Ⓢ dx.doi.org/10.1021/ic400251y

Unprecedented Tris-Phosphido-Bridged Triangular Clusters with 42 Valence Electrons. Chemical, Electrochemical and Computational Studies of their Formation and Stability

Tiziana Funaioli, Piero Leoni,* Lorella Marchetti, Alberto Albinati, Silvia Rizzato, Fabrizia Fabrizi de Biani, Andrea Ienco, Gabriele Manca, and Carlo Mealli*

This paper presents the synthesis and structural characterization of the unprecedented tris-phosphido-bridged compounds $Pt_3(\mu\text{-}PBu^t_2)_3X_3$ (X = Cl, Br, I), having only 42 valence electrons, while up to now analogous clusters typically have 44e⁻. The new species were obtained by an apparent bielectronic oxidation of the 44e⁻ monohalides $Pt_3(\mu\text{-}PBu^t_2)_3(CO)_2X$ with the corresponding dihalogen X_2. According to MO arguments, the unique stability of the 42e⁻ phosphido-bridged Pt_3 clusters can be attributed to the simultaneous presence of three terminal halides.

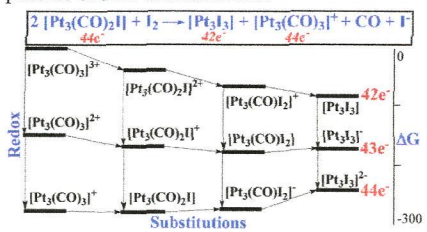

4648 Ⓢ dx.doi.org/10.1021/ic400273p

Molecular Dynamics Simulation of the Solid-State Topochemical Polymerization of S_2N_2

Teemu T. Takaluoma, Kari Laasonen, and Risto S. Laitinen*

Molecular dynamics simulations of the solid-state topochemical polymerization of four-membered S_2N_2 rings to $(SN)_x$ have been presented by involving DFT methods and periodic functions. The energetically most-favored reaction quickly propagates along *a* axis throughout the lattice. The structures of the polymer chains are in good agreement with that in the experimental crystal structure.

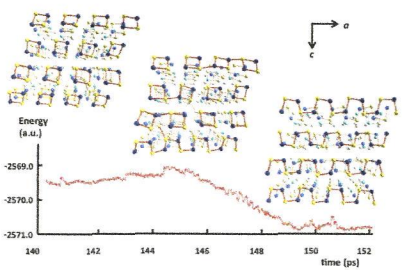

4658 Ⓢ dx.doi.org/10.1021/ic400275x

Lewis Acid Enhanced Axial Ligation of $[Mo_2]^{4+}$ Complexes

Brian S. Dolinar and John F. Berry*

We report here the synthesis, X-ray crystal structures, electrochemistry, and density functional theory single-point calculations of three new complexes: tetrakis(monothiosuccinimidato)dimolybdenum(II) [$Mo_2(SNO5)_4$, **1a**], tetrakis-(6-thioxo-2-piperidinonato)dimolybdenum(II) [$Mo_2(SNO6)_4$, **1b**], and chlorotetrakis(monothiosuccinimidato)pyridinelithiumdimolybdenum(II) [pyLi-$Mo_2(SNO5)_4$Cl, **2-py**].

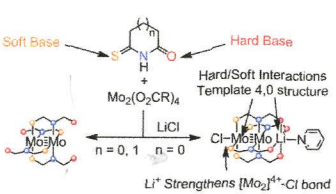

4668 Ⓢ dx.doi.org/10.1021/ic400280x

Generation of a High-Valent Iron Imido Corrolazine Complex and NR Group Transfer Reactivity

Pannee Leeladee, Guy N. L. Jameson,* Maxime A. Siegler, Devesh Kumar, Sam P. de Visser,* and David P. Goldberg*

A new high-valent iron terminal imide complex was generated by reaction of an iron(III) corrolazine with chloramine-T. Spectroscopic studies, DFT calculations, and reactivity patterns indicate an iron(IV) corrolazine-π-cation-radical assignment.

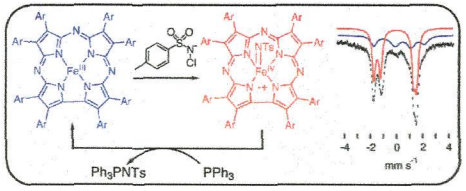

4683 Ⓢ dx.doi.org/10.1021/ic4002863

Guest-Triggered Zn^{II} Translocation and Supramolecular Nuclearity Control in Calix[6]arene-Based Complexes

Nicolas Bernier, Nicolas Menard, Benoit Colasson, Jean-Noël Rebilly,* and Olivia Reinaud*

A calix[6]arene bearing N-based coordination cores at each rim can bind selectively up to four Zn(II) ions. The macrocyclic cavity acts as a funnel for guest ligands and allows the supramolecular control of the metal complexes: depending on the guest, the binding site can switch from one rim to another in mononuclear complexes, and in polynuclear systems, the nuclearity can vary from three to four, while the coordination environment switches from O_h to T_d.

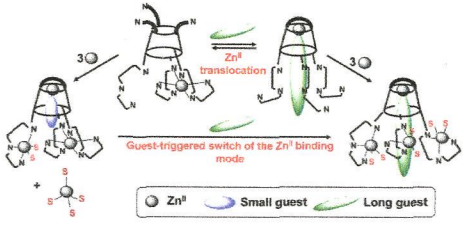

4692 dx.doi.org/10.1021/ic4002972

***closo*-Hydroborates from Liquid Ammonia: Synthesis and Crystal Structures of $[Li(NH_3)_4]_2[B_{12}H_{12}]\cdot 2NH_3$, $Rb_2[B_{12}H_{12}]\cdot 8NH_3$, $Cs_2[B_{12}H_{12}]\cdot 6NH_3$ and $Rb_2[B_{10}H_{10}]\cdot 5NH_3$**

Florian Kraus,* Monalisa Panda, Thomas Müller, and Barbara Albert

Ammoniates of the alkali metal *closo*-hydroborates are potentially storage materials for ammonia and hydrogen. The compounds were prepared as $[Li(NH_3)_4]_2B_{12}H_{12}\cdot 2NH_3$, $Rb_2B_{12}H_{12}\cdot 8NH_3$, $Cs_2B_{12}H_{12}\cdot 6NH_3$ and $Rb_2B_{10}H_{10}\cdot 5NH_3$ (4) for the first time and structurally characterized by low-temperature X-ray diffraction in the solid state.

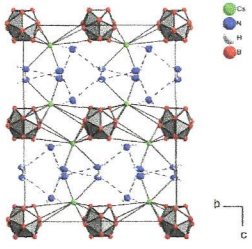

4700 Ⓢ dx.doi.org/10.1021/ic400335y

Multimetallic Complexes and Functionalized Nanoparticles Based on Oxygen- and Nitrogen-Donor Combinations

Saira Naeem, Angela Ribes, Andrew J. P. White, Mohammed N. Haque, Katherine B. Holt, and James D. E. T. Wilton-Ely*

Isonicotinic acid can be used as the basis of a range of heteronuclear multimetallic complexes. The same methodology can be employed to functionalize the surface of silver nanoparticles with ruthenium phosphine units.

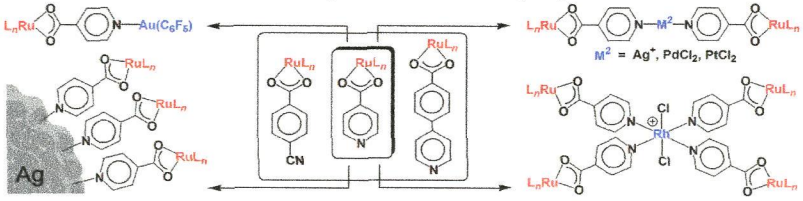

4714 Ⓢ dx.doi.org/10.1021/ic4003466

Phosphino-Boryl-Naphthalenes: Geometrically Enforced, Yet Lewis Acid Responsive P → B Interactions

Sébastien Bontemps, Marc Devillard, Sonia Mallet-Ladeira, Ghenwa Bouhadir, Karinne Miqueu,* and Didier Bourissou*

Three naphthyl-bridged phosphine-borane derivatives **2**-BCy_2, **2**-$BMes_2$, and **2**-BFlu, differing in the steric and electronic properties of the boryl moiety, have been prepared and characterized by spectroscopic and crystallographic means. The presence and magnitude of the P → B interactions have been assessed experimentally and theoretically. The naphthyl linker was found to enforce the P → B interaction despite steric shielding, while retaining enough flexibility to respond to the Lewis acidity of boron.

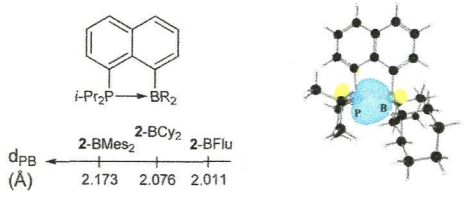

4721 Ⓢ dx.doi.org/10.1021/ic4003516

Switching Metal Ion Coordination and DNA Recognition in a Tandem CCHHC-type Zinc Finger Peptide

Angelique N. Besold, Abdulafeez A. Oluyadi, and Sarah L. J. Michel*

The DNA binding properties of Cys_2His_2Cys Zinc Finger Peptides can be modulated by single point mutations within the peptide sequence.